CHIN. PHYS. LETT. Vol. 36, No. 2 (2019) 027301

Phonon Limited Electron Mobility in Germanium FinFETs: Fin Direction Dependence *

Ying Jing(敬莹), Gen-Quan Han(韩根全)**, Yan Liu(刘艳), Jin-Cheng Zhang(张进成), Yue Hao(郝跃)
Key Laboratory of Wide Band-Gap Semiconductor Technology, School of Microelectronics, Xidian University, Xi'an 710071

(Received 26 October 2018)

We investigate the phonon limited electron mobility in germanium (Ge) fin field-effect transistors (FinFETs) with fin rotating within (001), (110), and (111)-oriented wafers. The coupled Schrödinger–Poisson equations are solved self-consistently to calculate the electronic structures for the two-dimensional electron gas, and Fermi's golden rule is used to calculate the phonon scattering rate. It is concluded that the intra-valley acoustic phonon scattering is the dominant mechanism limiting the electron mobility in Ge FinFETs. The phonon limited electron motilities are influenced by wafer orientation, channel direction, fin thickness $W_{\rm fin}$, and inversion charge density $N_{\rm inv}$. With the fixed $W_{\rm fin}$, fin directions of $\langle 110\rangle$, $\langle 1\bar{1}2\rangle$ and $\langle \bar{1}10\rangle$ within (001), (110), and (111)-oriented wafers provide the maximum values of electron mobility. The optimized $W_{\rm fin}$ for mobility is also dependent on wafer orientation and channel direction. As $N_{\rm inv}$ increases, phonon limited mobility degrades, which is attributed to electron repopulation from a higher mobility valley to a lower mobility valley as $N_{\rm inv}$ increases.

PACS: 73.50.−h, 73.50.Bk, 73.50.Dn DOI: 10.1088/0256-307X/36/2/027301

Germanium (Ge) metal-oxide-semiconductor field-effect transistors (MOSFETs) have attracted great interest because of their improved carrier mobility compared to Si devices[1−4] and the compatibility with CMOS technology.[5] Despite the low immunity to short-channel effects in Ge transistors due to relatively high dielectric constant (κ of 16 compared with 11.7 in silicon), electrostatic integrity can be improved using fully depleted device architectures, such as fin field-effect transistor (FinFET),[6] which shows a steeper sub-threshold slope, larger mobility and improved performance compared to planar transistor at low supply voltages ($V_{\rm DD}$).[7]

Apart from the electron and hole band structure, and the 3D electrostatic charging effects, the interactions of the free carriers with their environment (impurities, open surfaces, or lattice vibrations) strongly affect the performance of these devices. For example, electron-phonon scattering is expected to drastically deteriorate the ON current of devices with channel width below 5 nm.[8] Some attempts to include interface roughness[9] and electron-phonon scattering[10,11] have been demonstrated but they have almost always been limited to devices with transport along the [100] crystal axis. Other groups have reported that the orientation affects the Ge electron mobility,[12] but the device structure they studied is a single gate device whose quantization direction is always consistent with the direction normal to wafer, no matter how the channel direction changes. In Ge FinFETs, electrons are strongly confined in the fin plane, and electronic states and carrier transport characteristics change from those in bulk Ge. By adopting the vertical structure of the device (FinFETs), the quantization direction is not normal to wafer orientation anymore but normal to the fin plane.[13] In other words, we can achieve different quantization directions in one wafer orientation by changing the channel direction.

In this Letter, we present a comprehensive investigation of phonon limited electron mobility $\mu_{\rm ph}$ in Ge FinFETs, with the consideration of impacts of surface orientation, channel direction, and fin thickness $W_{\rm fin}$. The calculations of intra-valley acoustic phonon (AP), intra-valley optical and intervalley phonon (OP) scattering limited mobility are carried out.

The electron mobility is dependent on surface orientation due to the asymmetry of the carrier effective masses in Ge crystal lattice.[14,15] Our calculations were based on the effective mass framework and, therefore, to obtain the mobility in Ge fins along different directions we first computed the electron effective masses within arbitrarily surface orientations. In this calculation, we took $m_{\rm l} = 1.59m_0$ and $m_{\rm t} = 0.08m_0$ for Ge, where m_0 is the electron free-mass.[16−19] The approach that we used to obtain effective masses on the different combinations of wafer and fin direction are described in Ref. [20]. It is assumed that the electrostatic potential along transport and confinement directions is separable. Furthermore, the potential along transport direction changes slowly, so that the dipolar coupling will not happen. Based on these two assumptions, we can use two unitary operators to transform an arbitrarily oriented constant energy ellipsoid into a regular ellipsoid, whose principal axes are along the transport, width and confinement directions of the device.

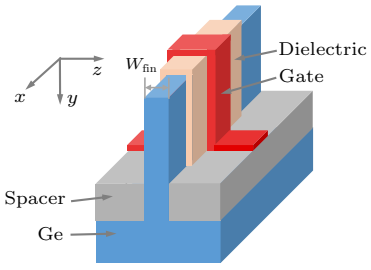

Fig. 1. The 3D schematic of Ge FinTFET used in the calculation.

Figure 1 presents the 3D schematic of Ge FinFET, and coordinate axes are also shown. For all our calculations, undoped fin channels were used.

*Supported by the National Natural Science Foundation of China under Grant Nos 61534004, 61604112 and 61622405.
**Corresponding author. Email: hangenquan@ieee.org
© 2019 Chinese Physical Society and IOP Publishing Ltd

Effective masses along confinement z direction m_z, DOS effective masses $m_{\rm DOS}$, and transport x direction m_x of Ge fins within (001), (110), and (111)-oriented surfaces are studied. For each surface orientation, m_z, $m_{\rm DOS}$ and m_x along all fin directions are computed. Figure 2 portrays the effects of surface orientation and fin direction on the values of effective masses at the L point. For (001) surface orientation, 0° and 90° correspond to [100] and [010] directions, respectively, for (110) orientation, 0° and 90° are taken along [001] and $[1\bar{1}0]$ directions, respectively, and for (111) orientation, the corresponding directions for 0° and 90° are $[\bar{1}10]$ and $[\bar{1}\bar{1}2]$, respectively. An obvious dependence of m_z, $m_{\rm DOS}$ and m_x on fin direction is observed. Ge has four equivalent valleys,[19] denoted by the valleys 1–4, which are along [111] $[11\bar{1}]$, $[\bar{1}11]$, and $[\bar{1}1\bar{1}]$ directions, respectively. For (001)-oriented surface, valleys 1 and 2 have the identical effective mass and valleys 3 and 4 have the same effective mass (Figs. 2(a), 2(d) and 2(g)). For (110)-oriented surface, valleys 1 and 2 are the same effective mass, whereas the other two are different (Figs. 2(b), 2(e) and 2(h)). For (111)-oriented surface, the four valleys exhibit different effective masses (Figs. 2(c), 2(f) and 2(i)).

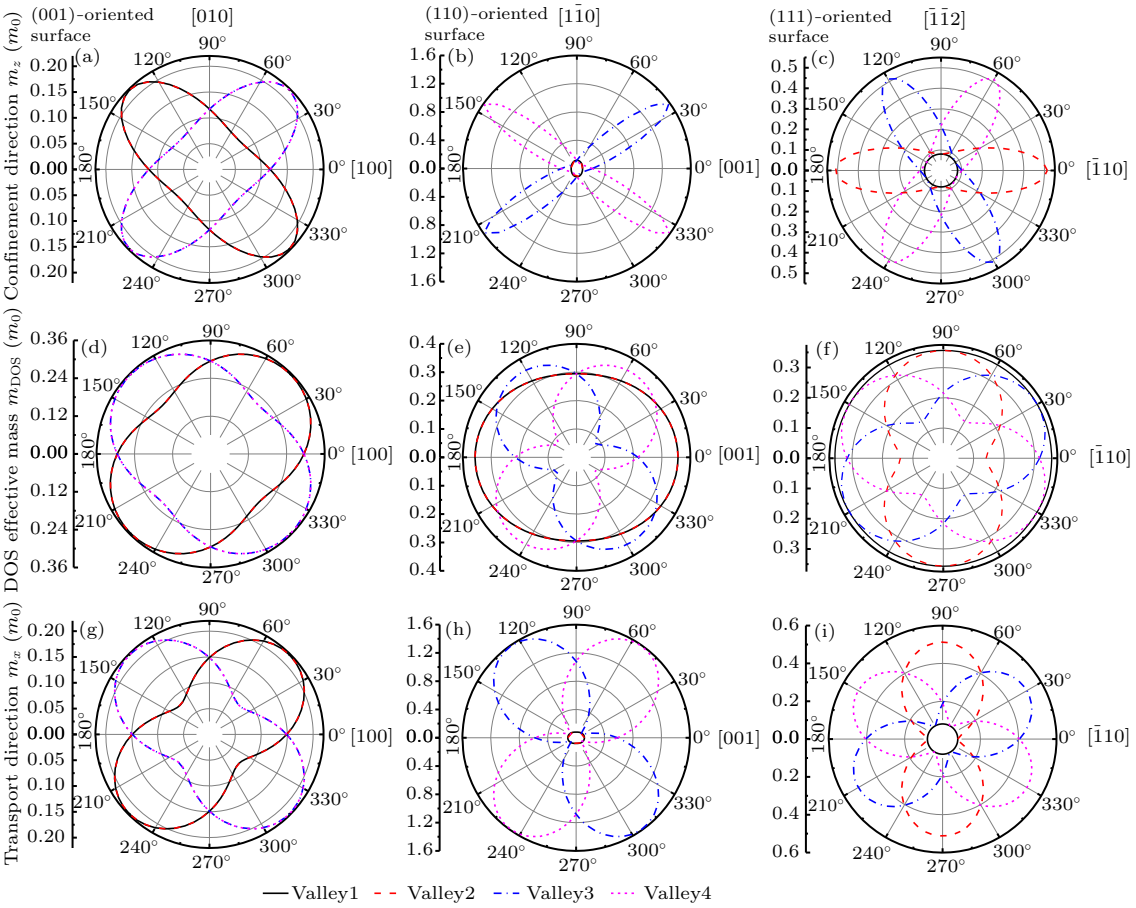

Fig. 2. Characteristics of m_z values within (a) (001), (b) (110) and (c) (111)-oriented surface, $m_{\rm DOS}$ values within (d) (001), (e) (110) and (f) (111)-oriented surface, m_x values within (g) (001), (h) (110) and (i) (111)-oriented surface.

From Fig. 2, we can see that m_z, $m_{\rm DOS}$ and m_x exhibit the anisotropic properties within the planes. In the following we only discuss the directions from 0° to 90°. For (001) surface, m_z, $m_{\rm DOS}$ and m_x all obtain their maximum values at 45° (Figs. 2(a), 2(d) and 2(g)). For (110) surface, in valleys 3 and 4, m_z achieves its maximum value at about 30° (Fig. 1(b)), while $m_{\rm DOS}$ and m_x obtain the maximum values at about 60° (Figs. 2(g) and 2(h)). Moreover, in valleys 1 and 2, the maxima of m_z, $m_{\rm DOS}$ and m_x are along 90°, 0° and 0°, respectively (Figs. 2(b), 2(g) and 2(h)). At 0° and 60°, m_z obtains the maximum value in (111) surface (Fig. 1(c)), $m_{\rm DOS}$ and m_x reach the maximum values at 30° and 90°, respectively, except valley 1 (Figs. 2(f) and 2(i)), and m_z, $m_{\rm DOS}$ and m_x of valley 1 in (111) surface are isotropic.

Electronic structures for the two-dimensional electron gas in Ge fins were obtained by solving the coupled Schrödinger–Poisson equation self-consistently within the envelope function based effective mass framework.[15,21] The phonons include acoustic and optical branches. For Ge, the phonon scattering processes consist of intra-valley acoustic phonons (AP), intra-valley optical and intervalley phonons (OP) scattering.[19] In our calculation, we assume the parabolic energy dispersion at the bottom of the Ge conduction band. The scattering probability of the intra-valley AP is[22]

$$\frac{1}{\tau_{\rm ac}^{(v,i)}} = \sum_j \frac{D_{\rm ac}^2 K_{\rm B} T m_d^{(v,j)}}{v_{\rm l}^2 \rho \hbar^3} F_{i,j}^{(v,v)} U(E - E_j^{(v)}), \quad (1)$$

where $D_{\rm ac}$ is the acoustic deformation potential,

$m_d^{(v,j)}$ and $E_j^{(v)}$ are the density of state effective mass and eigenvalue of jth sub-band in v-valley, respectively, v_l is the longitude sound speed, ρ is the germanium density, and $U(E)$ is the step function. The values of D_{ac}, v_l and ρ were set to 15 eV, 5400 m/s and 5323 kg/m, respectively.[19,23] The form factor is given by[22]

$$F_{i,j}^{(v,v')} = \int_0^\infty dz |\xi_{v,i}(z)|^2 |\xi_{v',j}(z)|^2, \qquad (2)$$

where $\xi_{v,i}(z)$ is the ith eigenfunction in the v-valley. For FinFET, the upper limit of the integral in Eq. (2) is W_{fin}. This is supposed to be a good approximation, because the relatively thick front- and back-oxide confine electrons into the Ge film very effectively.[22]

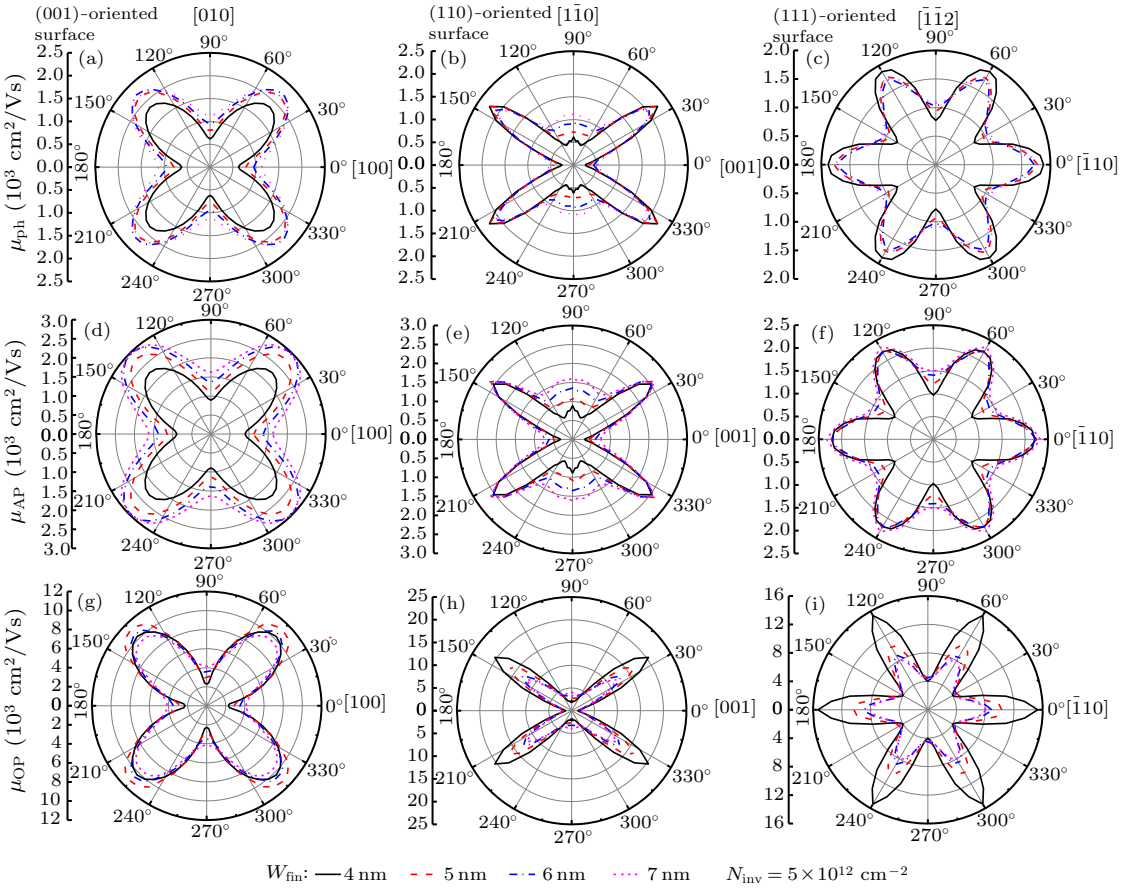

Fig. 3. The calculated μ_{ph}, μ_{AP} and μ_{OP} in Ge FinFETs with different W_{fin} rotating within the different surface orientations.

The scattering probabilities of the intra-valley optical and intervalley phonon are

$$\frac{1}{\tau_{op}^{(v,i)}(E)} = \sum_{v'} \sum_j \sum_m \frac{m_d^{(v',j)} D_{op,m}^2}{2\rho\hbar^2\omega_m} F_{i,j}^{(v,v')} g_m^{v,v'} \times \left[N_{op}(\hbar\omega_m) + \frac{1}{2} \mp \frac{1}{2} \right] \times \frac{1 - f_0(E \pm \hbar\omega_m)}{1 - f_0(E)} \times U(E \pm \hbar\omega_m - E_j^{v'}), \qquad (3)$$

where m denotes phonon modes, $D_{op,m}$ is the corresponding deformation potential of m-mode phonon, and $E_j^{(v')}$ is the eigenvalue of the final band in v'-valley. The factor $g_m^{v,v'}$ is the final sub-band degeneracy, given by the appropriate selection rules.[19] The phonon number, N_{op}, is obtained by the Bose–Einstein distribution. The upper and lower signs in Eq. (3) describe the phonon absorption and emission processes, respectively.[22]

Because different scattering mechanisms are involved in the calculations, the total momentum relaxation time (MRT) for a given sub-band $\tau_{total}^{(i)}$ is calculated by summing the inverse of the MRTs. The average MRT is finally obtained as[24]

$$\langle \tau_i \rangle = \frac{\int_{E_i}^\infty (E - E_i) \tau_{tot}^{(i)}(E) \frac{\partial f_0(E)}{\partial E} dE}{\int_{E_i}^\infty f_0(E) dE}. \qquad (4)$$

The phonon limited mobility μ_{ph} of the ith sub-band is calculated by $\mu_i = e\langle \tau_i \rangle / m_x^i$. The total effective mobility is the average of the sub-band mobilities weighted by the corresponding electron densities.

To obtain a better insight into the impacts of fin direction and surface orientation on μ_{ph} in Ge FinFETs, the mobility as a function of different combinations of wafer and fin direction are extracted with W_{fin} varying from 4 to 7 nm. Figure 3 shows the values of μ_{ph}

with different fin directions in (001), (110) and (111)-oriented surfaces at an $N_{\rm inv}$ of $5\times10^{12}\,{\rm cm}^{-2}$. In this case, $N_{\rm inv}$ is calculated as shown in Ref. [25], where $n(z)$ is the electron distribution, x^- is the position of the front interface between channel and gate oxide, $\mu_{\rm AP}$ is denoted as the intra-valley acoustic scattering limited mobility, and $\mu_{\rm OP}$ is the intra-valley optical and intervalley phonon scattering limited mobility.

Figures 3(a)–3(c) show the calculated total $\mu_{\rm ph}$ as a function of fin direction on (001), (110) and (111)-oriented surfaces, respectively. It is observed that $\mu_{\rm ph}$ has the strong dependence on fin direction and wafer orientation. Furthermore, it should be noticed that the directions of the maximum $\mu_{\rm ph}$ are not related to $W_{\rm fin}$ and the type of phonon scattering; that is, once the surface orientation is confirmed, the fin direction with maximum $\mu_{\rm ph}$ is fixed. For (001)-oriented surface, the maximum value of $\mu_{\rm ph}$ is achieved along the directions of [110] [$\bar{1}$10], [$\bar{1}\bar{1}$0] and [1$\bar{1}$0]. For (110)-oriented surface, the $\mu_{\rm ph}$ maxima are obtained in four directions: [1$\bar{1}$2], [1$\bar{1}\bar{2}$], [$\bar{1}$1$\bar{2}$] and [$\bar{1}$12]. However, for (111)-oriented surface, there are six directions, [$\bar{1}$10], [$\bar{1}$01], [0$\bar{1}$1], [1$\bar{1}$0], [10$\bar{1}$] and [01$\bar{1}$], along which $\mu_{\rm ph}$ reaches the maxima. It is noticed that values of $\mu_{\rm AP}$ are much smaller than those of $\mu_{\rm OP}$. In other words, the intra-valley acoustic phonon scattering is the dominating scattering mechanism in the phonon scattering. In addition, by comparing Figs. 1 and 3, we find that the directions for maximum $\mu_{\rm ph}$ are exactly consistent with those of m_z.

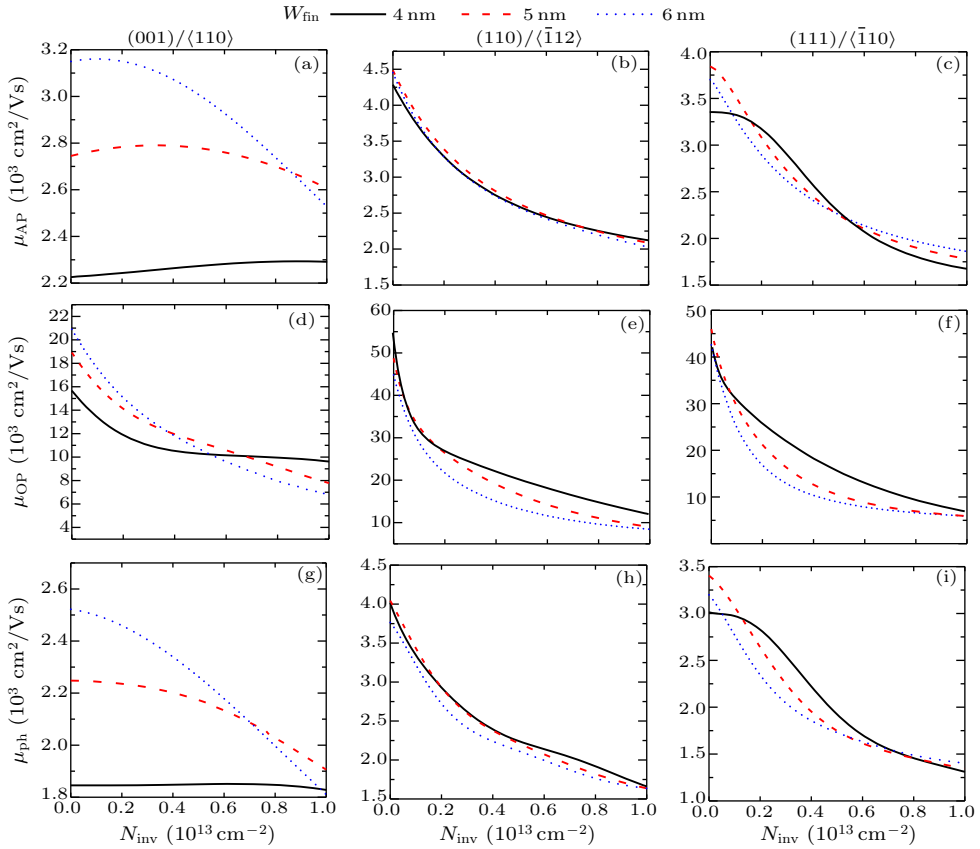

Fig. 4. The values of (a)–(c) $\mu_{\rm AP}$, (d)–(f) $\mu_{\rm OP}$ and (g)–(i) $\mu_{\rm ph}$ in Ge fins as a function of $N_{\rm inv}$ along the maximum mobility directions on various surface orientations. Here $W_{\rm fin}$ varies from 4 to 6 nm.

For $\mu_{\rm AP}$ along ⟨110⟩ directions within (001) surface (Fig. 4(a)), as $N_{\rm inv}$ increases, $\mu_{\rm AP}$ does not change monotonously. We can utilize Figs. 5(a)–5(c) to explain the trend of curves in Fig. 4(a). From Figs. 5(a)–5(c), we can find two reasons to explain the phenomena: the first is that the repopulation of electrons into lower $\mu_{\rm AP}$ valleys (dashed line), which makes $\mu_{\rm AP}$ decrease; the second is that the changes of $\mu_{\rm AP}$ in the four valleys (solid line). Because $N_{\rm inv}$ is small, the second reason is dominant, which makes $\mu_{\rm AP}$ increase because the values of $\mu_{\rm AP}$ in the four valleys all increase at small $N_{\rm inv}$. As $N_{\rm inv}$ goes up, the first reason is more important, which makes $\mu_{\rm AP}$ decrease. Based on this analysis, $\mu_{\rm AP}$ along ⟨110⟩ direction within (001) surface goes up, and then goes down as $N_{\rm inv}$ increases.

For the (110) and (111) cases, the relationship between $\mu_{\rm AP}$ and $N_{\rm inv}$ can be explained in the same way by Figs. 5(d) and 5(e). One is that the valley with lower $\mu_{\rm AP}$ has the lager electrons as $N_{\rm inv}$ increases, which leads to the decrease of $\mu_{\rm AP}$, and the other is that $\mu_{\rm AP}$ in the valley who has a larger mobility is reduced, which makes $\mu_{\rm AP}$ decrease. Therefore, along the directions for maximum mobility values within (110) and (111)-oriented surfaces, $\mu_{\rm AP}$ goes down as $N_{\rm inv}$ goes up.

For (110) and (111) cases, the relationship between $\mu_{\rm AP}$ and $N_{\rm inv}$ can be explained in the same way by Figs. 5(d) and 5(e). One is that the valley with lower $\mu_{\rm AP}$ has more electrons as $N_{\rm inv}$ increases, which leads to the decrease of $\mu_{\rm AP}$, and the other is that $\mu_{\rm AP}$ in the valley who has a larger mobility is reduced, which makes $\mu_{\rm AP}$ decrease. Therefore, along the directions

for maximum mobility values within (110) and (111)-oriented surfaces, μ_{AP} goes down as N_{inv} goes up.

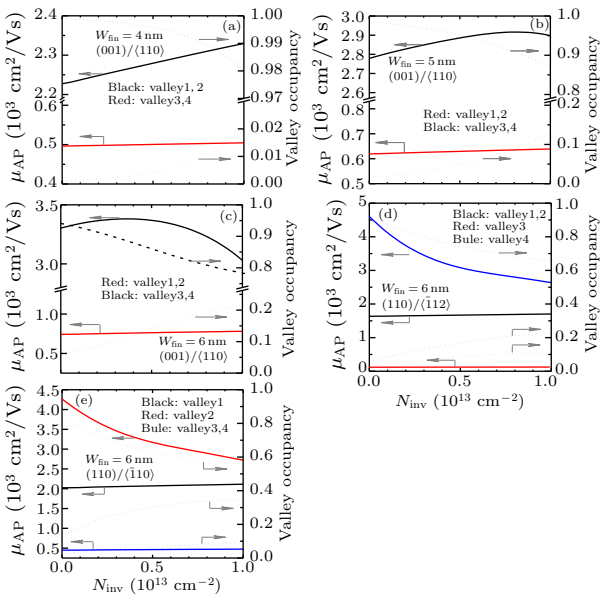

Fig. 5. The valley μ_{AP} and the corresponding occupancy on various surface orientations.

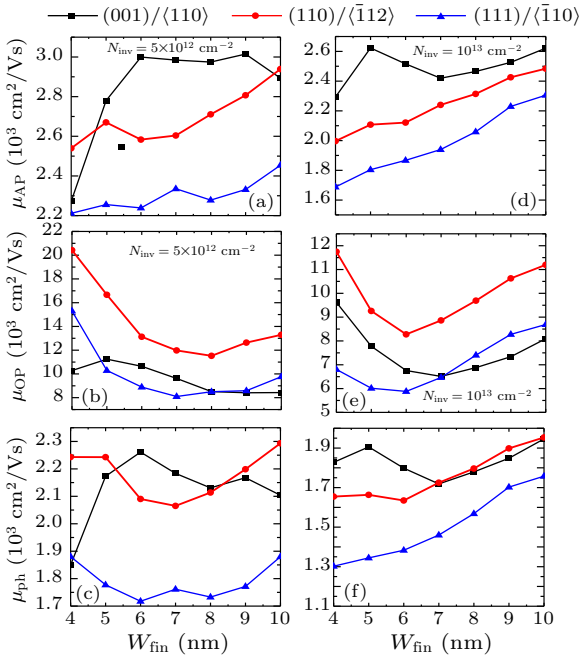

Fig. 6. The values of μ_{AP}, μ_{OP} and μ_{ph} at N_{inv} of (a)–(c) 5×10^{12} cm^{-2} and (d)–(f) 1×10^{13} cm^{-2} along the maximum mobility directions.

As shown in Figs. 4(d)–4(f), μ_{OP} decreases with increasing N_{inv} for all the surface orientations because the electrons in the larger μ_{OP} valley are reduced, which is the same reason as μ_{AP} in (110) and (111) case.

The total phonon limited mobility as a function of N_{inv} within three wafer orientations are shown in Figs. 4(g)–4(i). The curves are separated at different W_{fin} in (001) surface orientation, but it is not easy to distinguish from each other in the other two surface orientations.

Figure 6 shows the values of μ_{AP}, μ_{OP} and μ_{ph} as a function of W_{fin} along the directions for the maximum mobility values within different surface orientations, which are extracted at N_{inv} values of 5×10^{12} cm^{-2} and 1×10^{13} cm^{-2}. At an N_{inv} of 5×10^{12} cm^{-2}, for μ_{AP} (Fig. 6(a)), the (001) surface has the highest μ_{AP} in the range of W_{fin} = 5–10 nm, whereas the (110) surface has the highest μ_{AP} when W_{fin} is smaller than about 5 nm. The value of μ_{AP} in (111) surface orientation is always the lowest one in the range of W_{fin} = 4–10 nm. For μ_{OP} (Fig. 6(b)), the (110) surface always has the highest μ_{OP} in the range of 4–10 nm. Therefore, when the total phonon is taken into account, the (001) surface has the highest μ_{ph} in about 5–8 nm. Out of the range, the (110) surface has the highest μ_{ph} (Fig. 6(c)).

At N_{inv} of 10^{13} cm^{-2}, for μ_{AP} (Fig. 6(d)), the μ_{AP} (001) surface is always the highest one in the range of W_{fin} = 4–10 nm. For μ_{OP} (Fig. 6(e)), the (110) surface always has the highest μ_{OP} in the range of 4–10 nm. Therefore, when the total phonon is taken into account, μ_{ph} in the (001) surface is the highest one in the range of 4–7 nm. Out of the range, μ_{ph} in the (110) surface is the highest one (Fig. 6(f)).

Consequently, it is obvious that the mobility has strong dependence on W_{fin}, surface orientation and N_{inv}.

In summary, the phonon limited electron mobilities of Ge FinFET with different combinations of wafer orientation and fin direction are investigated via numerical simulation. With the fixed W_{fin}, fin directions of ⟨110⟩, ⟨1$\bar{1}$2⟩ and ⟨$\bar{1}$10⟩ on (001), (110) and (111)-oriented wafers provide the maximum values of μ_{ph}, respectively. The direction of maximum μ_{ph} is consistent with that of m_z. Furthermore, we compare the maximum μ_{ph} of three wafer orientations as a function of W_{fin}. We also find that at $N_{inv} = 5 \times 10^{12}$ cm^{-2}, μ_{ph} in the (001) surface is highest at W_{fin} = 5–8 nm. Out of the range, μ_{ph} in the (110) surface is highest. When it comes to $N_{inv} = 1 \times 10^{13}$ cm^{-2}, μ_{ph} in the (001) surface is highest in W_{fin} = 4-7 nm, and μ_{ph} in the (110) surface is highest about W_{fin} = 7-10 nm.

References

[1] Shang H et al 2002 *IEDM Tech. Dig.* **17.** **4** 441
[2] Wu N et al 2006 *IEEE Electron Device Lett.* **27** 479
[3] Amat E et al 2014 *IEEE Trans. Device Mater. Reliab.* **14** 344
[4] van Dal Mark J H et al 2014 *IEEE Trans. Electron Devices* **61** 430
[5] Kim J et al 2014 *IEEE Trans. Electron Devices* **35** 1185
[6] Poljak M et al 2012 *IEEE Trans. Electron Devices* **59** 1636
[7] Haensch W et al 2006 *IBM J. Res. Dev.* **50** 339
[8] Luisier M and G Klimeck et al 1950 *Phys. Rev. B* **80** 1
[9] Wang J et al 2005 *Appl. Phys. Lett.* **87** 043101
[10] Jin S et al 2006 *J. Appl. Phys.* **99** 123719
[11] Frey M et al 2008 *Proc. 38th ESSDERC* p 258
[12] Yang Y J et al 2007 *Appl. Phys. Lett.* **91** 102103
[13] Chang L et al 2004 *IEEE Trans. Electron Devices* **51** 1621
[14] Satô T et al 1971 *Phys. Rev. B* **4** 1950
[15] Stern F and Howard W E 1967 *Phys. Rev.* **163** 816
[16] Tanaka H et al 2014 *IEEE Trans. Electron Devices* **61** 1993
[17] Schäffler F 1997 *Semicond. Sci. Technol.* **12** 1515
[18] Niquet Y M et al 2009 *Phys. Rev. B* **79** 245201
[19] Jacoboni C and Reggiani L 1983 *Rev. Mod. Phys.* **55** 645
[20] Rahman A et al 2005 *J. Appl. Phys.* **97** 053702
[21] Jungemann C et al 1993 *Solid-State Electron.* **36** 1529
[22] Esseni D et al 2003 *IEEE Trans. Electron Devices* **50** 2445
[23] Low T et al 2004 *Appl. Phys. Lett.* **85** 2402
[24] Esseni D and Abramo A 2003 *IEEE Trans. Electron Devices* **50** 1665
[25] Gamiz F and Fischetti M V 2001 *J. Appl. Phys.* **89** 5478